Theoretical predictions for hexagonal BN based nanomaterials as electrocatalysts for the oxygen reduction reaction

Andrey Lyalin,[*abc‡] **Akira Nakayama,**[ab] **Kohei Uosaki,**[abd] **and Tetsuya Taketsugu**[abc]

Received Xth XXXXXXXXXX 20XX, Accepted Xth XXXXXXXXX 20XX
First published on the web Xth XXXXXXXXXX 200X
DOI: 10.1039/C2CP42907A

The catalytic activity for oxygen reduction reaction (ORR) of the pristine and defected hexagonal boron nitride (h-BN) monolayer and H-terminated nanoribbon have been studied theoretically using density functional theory. It is demonstrated that inert h-BN monolayer can be functionalized and become catalytically active by nitrogen doping. It is shown that energetics of adsorption of O_2, O, OH, OOH, and H_2O on N atom impurity in h-BN monolayer (N_B@h-BN) is quite similar to that known for Pt(111) surface. The specific mechanism of destructive and cooperative adsorption of ORR intermediates on the surface point defects is discussed. It is demonstrated that accounting for entropy and zero-point energy (ZPE) corrections results in destabilization of the ORR intermediates adsorbed on N_B@h-BN, while solvent effects lead to their stabilization. Therefore, entropy, ZPE and solvent effects partly cancel each other and have to be taken into account simultaneously. Analysis of the free energy changes along the ORR pathway allows us to suggest that N-doped h-BN monolayer can demonstrate catalytic properties for ORR under condition that the electron transport to the catalytically active center is provided.

1 Introduction

Oxygen reduction reaction (ORR) is a key process that allows fuel cells to operate. Currently the most efficient catalysts for ORR are based on precious metals, such as platinum.[1–3] The relatively low efficiency of the known ORR catalysts, voltage losses at the cathode, the high cost and limited resources of platinum prevent the wide use of fuel cells in practical applications. Therefore, many efforts are underway to develop the efficient and non-precious metal ORR catalyst. The research in this direction can be divided into two groups - (i) understanding the mechanisms of ORR on Pt catalyst and improving characteristics of Pt based catalysts; (ii) attempts to develop alternative Pt-free catalysts using more abundant elements. In the first group a progress has recently been achieved by using platinum alloys with transition metals, like Fe, Ni, Co, Pd, and Ru, or considering a thin films of Pt deposited on various metal or carbon supports.[3–8] In the second group ORR activity has been found in some of the transition metal oxides and carbides, effective polyaniline bases catalysts and carbon alloys doped with a certain amount of N and B atoms.[3,9–19] Recently, it has been reported that carbon-based nanomaterials, such as graphene clusters doped with nitrogen or nitrogen and boron atoms (carbon alloy catalyst) demonstrate high ORR activity.[11–14,16–20] Boron atom stabilizes the N impurity nearby the edge of the graphene cluster and make it more reactive.[16] Therefore, the N-B doped carbon alloys can be considered as a good candidate for an effective and cheap ORR catalyst. Unfortunately, the mechanism of ORR and even clear identification of the ORR active sites in the N-B doped carbon alloys remain elusive.

Thus, it was demonstrated that in the case of N doped graphene clusters the active sites for ORR are C atoms on graphene-like zigzag edges if a graphite-like N atom is located near the edge.[14] This position of N impurity is not stable thermodynamically in comparison with the pyridinum-like configuration of N which in turn is not active for ORR.[14] It was shown that in the case of the N-B doped graphene clusters the ORR active sites are boratabenzene-like B atoms located nearby the graphite-like N atoms.[16] In both cases the graphite-like N atom nearby the zigzag edge of the cluster activates the neighboring C and B atoms. However, ref. 18 demonstrates that namely pyridine-like and pyrrole-like active centers possess electrocatalytic property for ORR in the case of N-graphene clusters $C_{45}NH_{20}$ and $C_{45}NH_{18}$. Moreover, it was shown that the N doped graphene monolayer can also possesses ORR activity.[17] In the latter case, the catalytic reaction occurs not at the edge of the finite cluster or one-dimensional carbon nanoribbon, but on the surface of the N

[a] *Center for Strategic Utilization of Elements, Graduate School of Science, Hokkaido University, Sapporo 060-0810, Japan. E-mail: lyalin@mail.sci.hokudai.ac.jp*
[b] *Department of Chemistry, Faculty of Science, Hokkaido University, Sapporo 060-0810, Japan.*
[c] *Elements Strategy Initiative for Catalysts and Batteries (ESICB), Kyoto University, Katsura, Kyoto 615-8520, Japan.*
[d] *International Center for Materials Nanoarchitechtonics (WPI-MANA), National Institute for Materials Science (NIMS), Tsukuba 305-0044, Japan.*
‡ On leave from: V. A. Fock Institute of Physics, St Petersburg State University, 198504 St Petersburg, Petrodvorez, Russia

doped graphene sheet. It was demonstrated that the catalytic activity of the N doped graphene monolayer decreases with increase in the local concentration of N atoms.[17] Thus, structure where N atoms are separated by three C atoms is more active if compared with the structure with two C atoms between N atoms.[17] On the other hand, as it was discussed above the co-doping of N-graphene clusters with B atoms promotes their ORR activity. Therefore, one can suggest that the consequent substitution of C atoms in the N-graphene by B atoms might result in increase of the ORR activity. In the extreme case when all C atoms in graphene are substitued by N and B one can obtain the h-BN monolayer, which has geometrical structure similar to graphene. Recently a promising 'chemical blowing' method has been developed for mass production of BN nanosheets. Such material is consideably cheaper than Pt and consists of abundant elements.[21,22] Can h-BN possess any catalytic activity for ORR? The answer to this question can open the way for development of the principally new class of ORR catalysts, based on materials that traditionally were believed to be inert.

In the present paper we demonstrate theoretically that nanomaterials mainly consisting of B and N atoms such as h-BN can possess catalytic activity for ORR. We demonstrate that among all adsorption sites considered on the surface of the pristine and defected h-BN monolayer as well as at the H-terminated edges of h-BN nanoribbons the N impurity defect in h-BN monolayer (N_B@h-BN) can be a good candidate for ORR active center. It is shown that adsorption energies of O_2 and other ORR intermediates, such as O, OH, and OOH on the N doped h-BN monolayer are similar to those known for Pt(111) surface. This finding allows us to suggest that N_B@h-BN center can possess catalytic properties for ORR similar to Pt.

2 Methods

In the present work we use a model approach introduced by Nørskov[23] and described in details by Keith and Jacob.[24–26] In this approach in order to describe the whole ORR process one should calculate the adsorption energies of ORR intermediates on the model catalyst. The calculations are carried out using density-functional theory (DFT) with the gradient-corrected exchange-correlation functional of Wu and Cohen (WC).[27] The WC functional provides a good compromise adequately describing energetics of covalent and noncovalent bonds in oxygen and hydrogen molecules, ORR intermediates, as well as h-BN lattice constants and electronic structure.[28] Double-ζ plus polarization function (DZP) basis sets are used to treat the $2s^22p^1$, $2s^22p^3$, and $2s^22p^4$ valence electrons of B, N, and O atoms, respectively.[29,30] Triple-ζ plus polarization function (TZP) basis set is used for H atom. Basis set for hydrogen was optimized with the use of the Nelder-Mead simplex method[31] according to the procedure described in ref. 30. The core electrons are represented by the Troullier-Martins norm-conserving pseudopotentials[32] in the Kleinman-Bylander factorized form.[33] All calculations have been carried out with the use of the SIESTA package.[34–36] Periodic boundary conditions are used for all systems, including free molecules. In the latter case the size of a supercell was chosen to be large enough to make intermolecular interactions negligible. The h-BN lattice has been optimized using the Monkhorst-Pack[37] $10\times10\times4$ k-point mesh for Brillouin zone sampling. The calculated lattice parameters a = b = 2.504 Å and c = 6.656 Å are in excellent agreement with the experimental values of a = b = 2.524 $\pm$ 0.020 Å and c = 6.684 $\pm$ 0.020 Å, reported in ref. 38. The h-BN monolayer is represented by the slab containing 6×6 unit cells (36 units of BN per slab). The periodically replicated slabs are separated by the vacuum region of 15 Å to avoid interaction between h-BN layers. All atoms in the h-BN slab are fully relaxed. Only the Γ point is used for sampling the Brillouin zone of the slab due to the large size of the supercell. The energy cutoff of 200 Ry is chosen to guarantee convergence of the total energies and forces. A common energy shift of 10 meV is applied. The self-consistency of the density matrix is achieved with a tolerance of 10^{-4}. For geometry optimization the conjugate-gradient approach was used with a threshold of 0.02 eV Å^{-1}. To validate our approach and choice of WC functional we have calculated the dissociation energies and interatomic distances for O_2 and H_2 diatomic molecules. Our calculations demonstrate that the dissociation energy, D_e, and bond length in O_2 (5.88 eV, 1.24 Å) and H_2 (4.53 eV, 0.75 Å) are in a good agreement with experimental data O_2 (5.23 eV, 1.21 Å) and H_2 (4.74 eV, 0.741 Å).[39] We have also calculated geometries and energetics of water monomer and dimer to illustrate the feasibility of our approach for describing water molecules and hydrogen bonds. The calculated OH bond length and HOH angle in H_2O (0.97 Å, 103.8°) are in good agreement with experimental data (0.957 Å, 104.52°).[40] The calculated dissociation energy, D_e, and the OO bond length in water dimer (0.26 eV, 2.82 Å) are in excellent agreement with the experimental results (0.236 eV, 2.976 Å)[41,42] and results of *ab initio* CCSD(T) calculations (0.218 eV, 2.921 Å).[43] In order to obtain the most stable configuration of the adsorbed O_2 and ORR intermediates we have created a large number of starting geometries by adding O_2, OOH, O and OH species in different nonequivalent positions (up to 30 in each case) at the edges of h-BN nanoribbon and on the surface of the pristine and defected h-BN. The starting structures have been optimized without any geometry constraints. The similar approach has been successfully used in our previous works to study adsorption and dissociation of O_2, H_2, and C_2H_4 molecules on the free and supported gold clusters[44–51] and cluster structure optimization.[52–54] The atoms in molecules method of Bader (AIM) has been used for

charge analysis.[55,56]

3 Results and discussion

3.1 Low-dimensional h-BN based structures

The h-BN lattice has a layered hexagonal structure which is very similar to graphite. The planar networks of B_3N_3 hexagons are regularly stacked on top of each other.[57] Due to the partially ionic character of the B–N bonding, the B atoms in one layer are located on top of the N atoms of the neighboring layers and vice versa. In graphite, however, layers are shifted in respect to each other, thus C atoms in one layer are located on top of the middle of the hexagonal ring in the neighboring layers. Both graphite and h-BN materials are strongly bonded within the layers, while interaction between the layers is weak. In spite of similarities in structures, the physical and chemical properties of graphite and h-BN are very different. Thus, graphite has a black color and possess electron conductivity, while h-BN is a white color dielectric with a wide band gap of 5-6 eV and high thermal and chemical stability. It is unlikely that O_2 and other ORR intermediates can be adsorbed on the h-BN surface. It is even more unlikely that O_2 can be activated on such a support. Moreover, catalyst for a fuel cell cathode must provide an electron transport to the active sites of ORR. This is impossible task to do, when catalyst has dielectric properties. These are the reasons why h-BN has never been considered as ORR catalyst for fuel cells. However, electronic properties of the low-dimensional h-BN systems such as h-BN monolayer and h-BN nanoribbons can differ considerably from those known for the h-BN bulk. Recently, it was shown, that the h-BN nanoribbons become semiconducting due to doping-like conducting edge states and vacancy defects.[58] The band gap in a h-BN monolayer can be considerably reduced by vacancy and impurity defects[58,59] or by decorating BN sheet with hydrogen atoms.[60] Recently Geim and Novoselov with colleagues demonstrated an electron tunneling effect through h-BN sheets deposited on a gold substrate.[61] Moreover, it was demonstrated experimentally that h-BN monolayer deposited on the transition metal support can be a conductor under certain conditions.[62] Theoretical calculations confirm that the electronic properties of h-BN monolayer supported on 3d, 4d and 5d transition metal surfaces can be strongly modified as a result of mixing of the d_{z^2} metal orbitals with N-p_z and B-p_z orbitals of h-BN monolayer.[63] It is important to note, that adsorption energies of ORR intermediates can be strongly affected by the density of electronic states (DOS) near the Fermi level. Therefore metal substrate can influence catalytic reaction on h-BN surface. It can be also possible to tune adsorption energies of ORR intermediates on h-BN by the metal support to design the most effective catalyst. This suggestion requires further investigation that goes far beyond the aims of the present study. However, in order to investigate the interconnection between electronic structure and catalytic activity of the pristine and defected h-BN structures we have performed analysis of the density of electronic states of the considered systems.

In the present paper we study ORR activity of pristine and defected h-BN monolayer and the H-terminated h-BN nanoribbon without addressing the conductivity problem directly. The effect of transition metal support on ORR activity of h-BN monolayer (nanomesh) and possibility to provide an electron transport to the catalytically active centers on the h-BN surface will be reported in a further publication.

3.2 Adsorption and activation of O_2 on the h-BN based structures

Adsorption and activation of O_2 on the catalytic material is the first and the most important step for ORR. In the present work we study several possible sites for O_2 adsorption, including pristine h-BN monolayer, h-BN monolayer with four simplest types of point defects, such as boron vacancy (V_B), boron impurity (B_N), nitrogen vacancy (V_N), and nitrogen impurity (N_B), as well as the H-terminated zigzag edge of h-BN sheet represented by the h-BN nanoribbon with a finite width of 9.44 Å. The considered structures are schematically shown in Fig. 1.

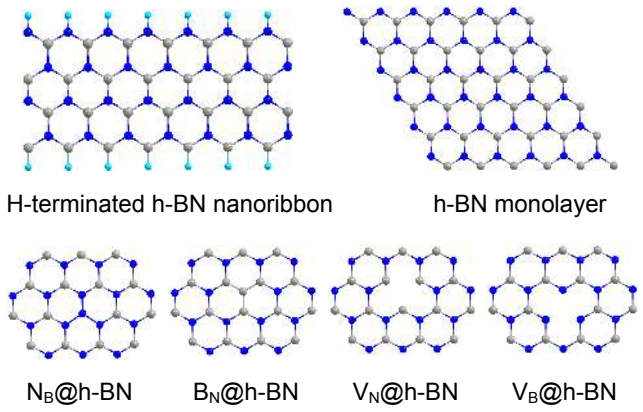

Fig. 1 Surface models: top view of the H-terminated h-BN nanoribbon p(7) slab with a width of 9.44 Å; h-BN monolayer p(6x6) slab; schematic presentation of the h-BN monolayer with nitrogen impurity (N_B), boron impurity (B_N), nitrogen vacancy (V_N), and boron vacancy (V_B) defects (only part of the slab is shown). Boron and nitrogen atoms are colored gray and blue, respectively, while hydrogen atoms are colored light blue.

The relative stability of various point defects in h-BN has been intensively investigated. It was demonstrated N_B and B_N impurity defects have low formation energies, comparable to those of the vacancies V_N and V_B.[64,65] Thus, it was

found that N_B is the most stable defect in h-BN under N-rich conditions followed by the nitrogen vacancy.[64] This is consistent with experimental findings of large concentrations of nitrogen interstitials and vacancies, and of the trapping of nitrogen in the hexagonal phase of BN thin films grown by ion-bombardment assisted deposition techniques; see, ref. 64 and references therein. The relative stability of particular type of defects in h-BN often depends on the experimental conditions. Therefore, in the present work we study only the simplest and the most stable point and linear (H-terminated zigzag edge) defects in h-BN.

To gain more insight into the electronic structure of the considered h-BN based systems we have calculated the spin polarized DOS which are presented in Fig. 2.

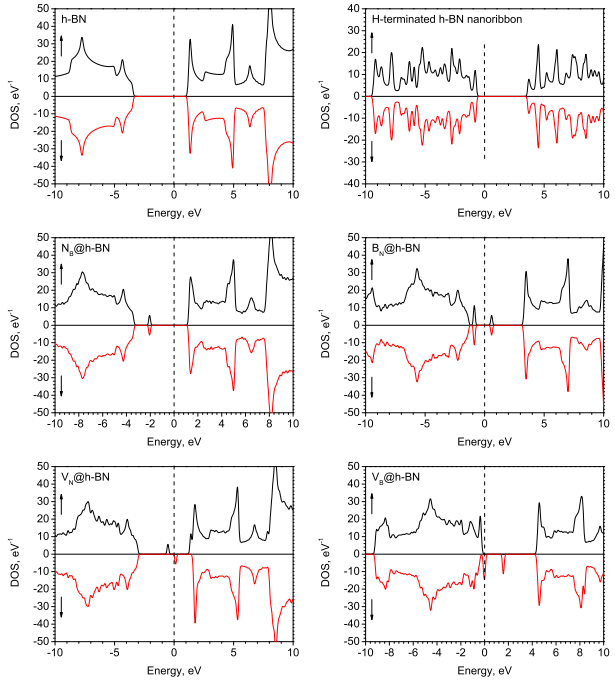

Fig. 2 Spin polarized density of electronic states (DOS) calculated for the defect free h-BN monolayer, H-terminated h-BN nanoribbon and h-BN monolayer with N_B, B_N, V_N, and V_B point defects. The location of the Fermi level is indicated by a dashed vertical line at 0 eV. Arrows directed up and down indicate the up-spin and down-spin DOS, respectively. A Gaussian broadening of half-width 0.1 eV has been used.

The detailed analysis of the electronic structure of nitrogen, boron and carbon impurity as well as nitrogen and boron vacancy defects in h-BN monolayer has been recently reported in ref. 59. Our results are in a very good agreement with data presented in ref. 59. Our calculations demonstrate that the defect-free h-BN monolayer has a wide band gap of 4.61 eV. Experimental values of the band gap energy for solid h-BN are widely dispersed in the range between 3.6 and 7.1 eV depending on the experimental method.[66] Recent results obtained from the analysis of laser-induced high-resolution fluorescence excitation spectrum of h-BN powder have determined the band gap energy of the solid h-BN: E_g = 4.02 $\pm$ 0.01 eV.[66] In the case of H-terminated h-BN nanoribbon the band gap depends on the ribbon width, decreasing with increase in width. The value of the band gap calculated for the nanoribbon of a width 9.44 Å is 4.39 eV which is slightly smaller if compared with the band gap of the defect-free h-BN monolayer. Figure 2 demonstrates that incorporation of N_B, B_N, V_N, and V_B point defects in h-BN monolayer result in a significant change of the electronic structure of h-BN and appearance of the defect levels in the band gap.[59] Nitrogen impurity introduces occupied level located 1.29 eV above the edge of the conductivity band, decreasing the bang gap in N_B@h-BN to 3.27 eV. Boron impurity defect induces two nearly degenerated occupied levels and one unoccupied level in the forbidden zone decreasing the band gap in B_N@h-BN to 1.45 eV as shown in Fig. 2. The results of our calculations show that V_N and V_B vacancy defects in h-BN monolayer induce spin polarization of DOS. The V_N defect introduces two levels in the forbidden zone, one of which (spin-up) is occupied and another one (spin-down) is located just above the Fermi level. The energy difference between two defect levels in V_N@h-BN is 0.65 eV. The energy gaps calculated for spin-up (E_g^{up}) and spin-down (E_g^{down}) electrons in V_N@h-BN are 1.83 eV and 1.44 eV, respectively. It is seen from Fig. 2 that V_N@h-BN monolayer possesses properties of n-type semiconductor for spin-up electrons, and p-type semiconductor for spin-down electrons. The boron vacancy V_B defect in h-BN is one of the most interesting defects as it induces occupied (spin-up) and unoccupied (spin-down) levels in the vicinity of the Fermi level, and unoccupied spin-down level located 1.61 eV above the Fermi level. Therefore V_B defect in h-BN behaves as a triple acceptor of electrons.[59] The strong acceptor ability of V_B defect in h-BN has been also reported in our recent works.[50,51] Moreover, formation of the defect states around the Fermi level can result in appearance of the electronic conductivity in V_B@h-BN. Similar effect has been found experimentally for h-BN nanoribbons with boron vacancy defects.[58] The features of electronic structure in defected h-BN systems can affect the process of O_2 adsorption and activation. The catalytic activation of the adsorbed O_2 is related to an electron transfer from the support to the oxygen anti-bonding $2\pi^*$ orbital. Therefore it is unlikely that O_2 can be activated on the defect free h-BN monolayer as it has a wide band gap with no electron density nearby the Fermi level. On the other hand presence of the defect levels nearby the Fermi level in defected h-BN can result in catalytic activation of O_2. However, analysis of the electronic structure of BN based nanosystems can not give information about the values

of binding energies of O_2 to defects in h-BN. Therefore we perform systematic analysis of O_2 adsorption on h-BN systems.

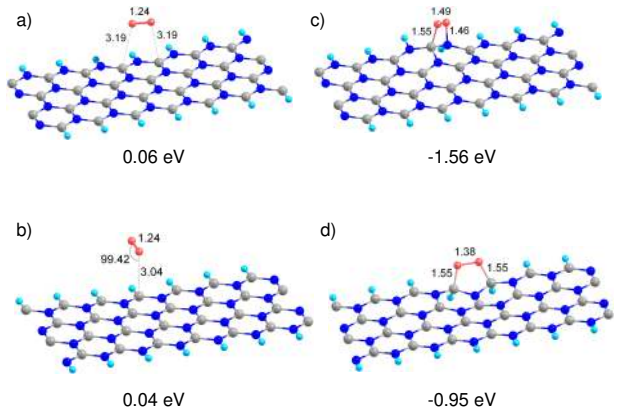

Fig. 3 The most stable (left) and the first activated (right) configurations of an oxygen molecule adsorbed on the H-terminated edges of h-BN nanoribbon containing pyridinium-like N (top row) and boratabenzene-like B (bottom row) atoms. The interatomic distances are given in Angstroms and angles are given in degrees. Binding energy of O_2 to h-BN nanoribbon is indicated at the bottom.

It was shown that a BN pair dopant at the edge of carbon sheet can serve as an active site for adsorption, catalytic activation and further reduction of O_2.[16] The edges of h-BN nanoribbons consist only of BN pairs and hence might demonstrate promising activity for ORR. Our calculations demonstrate, however, that O_2 binds weakly to the H-terminated edges of the model h-BN nanoribbon and remains non-activated. Figures 3a) and 3b) demonstrate that O−O bond in the adsorbed O_2 is oriented parallel to the h-BN nanoribbon edge containing pyridinium-like N atoms and perpendicular to the edge containing boratabenzene-like B atoms with the binding energy of 0.06 eV and 0.04 eV, respectively. Here, the binding energy of O_2 to the h-BN nanoribbon is defined as

$$E_b(\mathrm{O_2/h{-}BN}) = E_{tot}(\mathrm{O_2}) + E_{tot}(\mathrm{h{-}BN}) - E_{tot}(\mathrm{O_2/h{-}BN}), \quad (1)$$

where E_{tot}(O_2/h-BN) denotes the total energy of the O_2/h-BN system, while E_{tot}(O_2) and E_{tot}(h-BN) are the total energies of the non-interacting O_2 and h-BN nanoribbon, respectively. It is unlikely that such weakly adsorbed and non-activated O_2 can participate in ORR. On the other hand the activated configurations of the adsorbed O_2 (Figures 3c) and 3d)) are metastable, with the binding energies to the pyridinium-like and boratabenzene-like edges of h-BN nanoribbon of -1.56 eV and -0.95 eV, respectively. The negative sign of E_b indicates that adsorbant is not stable towards desorption from the support. Therefore the H-terminated edge of the considered h-BN nanoribbon does not likely possess catalytic activity for ORR in contrast to the BN defect pair at the edge of graphite sheet.

Let us now consider adsorption of O_2 on h-BN monolayer with simple point defects. Figure 4 presents the optimized geometries of O_2 adsorbed on the defect-free h-BN monolayer and h-BN monolayer with N_B, B_N, V_N, and V_B defects. It is seen from Fig. 4 that O_2 adsorbs in a configuration when the O−O bond is oriented parallel to the surface plane in all considered cases with an exception of B_N@h-BN support. In the latter case O_2 adsorbs on top of B impurity atom and inclined from the surface normal. Note that defected h-BN monolayer possesses structural relaxations upon O_2 adsorption. Our calculations demonstrate that molecular oxygen physisorbed on the defect-free h-BN monolayer in a triplet spin state with the binding energy of 0.06 eV, and remains catalytically non-activated. However, O_2 chemisorbs on N_B, B_N, V_N, and V_B point defects in a singlet spin state with E_b= 0.24 eV, 1.62 eV, 3.10 eV, and 1.96 eV, respectively. Interaction of O_2 with the point defects in h-BN monolayer results in activation of the adsorbed O_2 and weakening of the O−O bond. Figure 4 demonstrates that the O−O bond length in O_2 adsorbed on N_B@h-BN, B_N@h-BN, and V_N@h-BN support is enlarged similar to the superoxide state of oxygen (the O−O bond distances in O_2^- is 1.33 Å[67]). In the case of O_2 adsorption on the V_B defect in h-BN monolayer oxygen molecule is partially dissociated with the distance between O atoms of 1.79 Å. Can this adsorbed O_2 be active for ORR? To answer this question let us compare the binding energies of O_2 to the considered BN based systems and to the Pt(111) surface. Of course Pt(111) is not the ideal catalyst for ORR, but such a comparison can give a clue whether or not BN based nanomaterials can have catalytic properties similar to Pt. The low-temperature thermal desorption spectroscopy and electron energy-loss spectroscopy have determined the low-coverage E_b of O_2 to Pt(111) to be 0.3-0.5 eV; see, e.g., refs. 68–70 and references therein. The DFT calculations of a gas phase adsorption of O_2 on a Pt_{35} cluster, as a model for Pt(111) surface give the value of E_b= 0.49 eV.[26] Earlier theoretical studies of O_2 adsorption on the model Pt(111) surface gives values of the binding energy to a surface to be 0.65-0.72 eV for peroxo-like state and 0.53-0.68 eV for superoxo-like state of the adsorbed O_2.[71,72] In general the ideal E_b of O_2 to a good catalytic material for ORR should be as small as possible, but large enough to prevent O_2 to drift away or desorb from the catalytic center. We can also add that the heats of formation of the adsorbed O_2 should be smaller than the heats of formation of OOH intermediate on the surface, otherwise ORR will not be energetically favorable process. Although O_2 adsorbed on B_N@h-BN, V_N@h-BN, and V_B@h-BN is catalytically activated, the binding energy of O_2 to the support is too large. Therefore, h-BN monolayer with B_N, V_N, and V_B defects can not be a good catalyst for ORR. On the other hand, in the case of O_2 adsorption on the N_B

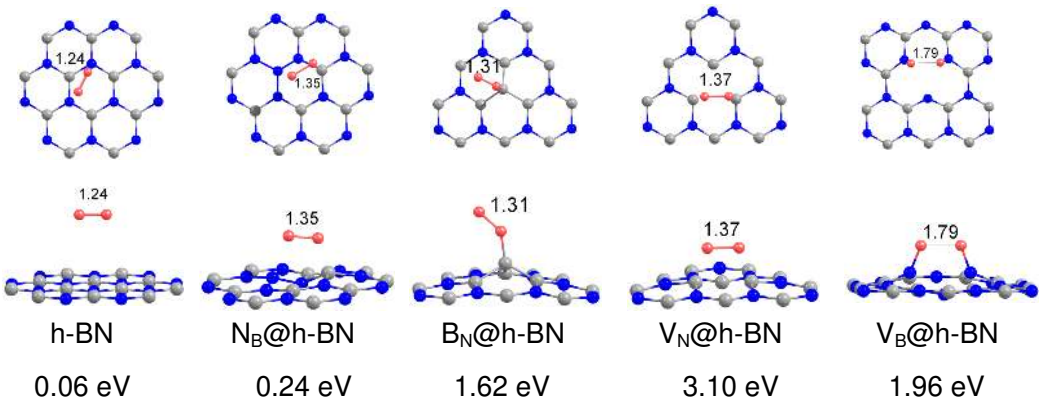

Fig. 4 The most stable configurations of an oxygen molecule adsorbed on the defect-free h-BN monolayer and h-BN monolayer with N_B, B_N, V_N, and V_B point defects. The interatomic distances are given in Angstroms. Binding energy of O_2 to h-BN monolayers are indicated at the bottom. Only part of the slab is shown.

impurity defect, the oxygen molecule is activated and weakly bounded to the surface. It is interesting that binding energy of O_2 to N_B@h-BN is similar to that known for O_2 adsorbed on the Pt(111) surface. Therefore, one can suggest that the N impurity in h-BN monolayer can play a role of an active center for ORR. In order to check this suggestion we calculate binding energies of ORR intermediates, such as O, OOH, OH and H_2O to V_N@h-BN center.

3.3 Adsorption of the ORR intermediates on the h-BN monolayer with N impurity defect

Figure 5 presents the most stable configurations of O_2^*, OOH^*, O^*, OH^*, and H_2O^* adsorbed on the h-BN monolayer with N impurity defect. Here and below molecules adsorbed on the surface are marked by asterisk (*). O_2 adsorbs on N_B@h-BN in the vicinity of the B atom located nearby the N_B impurity. Adsorption of O_2 results in the local distortion of the h-BN lattice. Thus, the B atom localized in the vicinity of the adsorbed O_2 protrudes above the surface plane by ~ 0.4 Å.

The binding energy of O_2 to N_B@h-BN is 0.24 eV. The adsorbed O_2^* is strongly activated with the O−O bond length increased to 1.35 Å. In order to clarify mechanism of O_2 activation on N_B@h-BN we present analysis of the partial density of electronic states (PDOS) projected on B and N atoms (solid line) and O_2 (dashed line) calculated for noninteracting N_B@h-BN monolayer and free O_2 (Fig. 6a); as well as O_2 adsorbed on N_B@h-BN (Fig. 6b). As it was discussed above the N_B defect in h-BN monolayer induce an occupied level in the forbidden zone, as it is shown in Fig. 6a. This level localized at the N_B defect and has p_z character. Oxygen molecule possesses the occupied up-spin antibonding $2\pi^*$ orbital which is located below the Fermi level and the unoccupied down-spin $2\pi^*$ orbital above the Fermi level. Adsorption of O_2 on

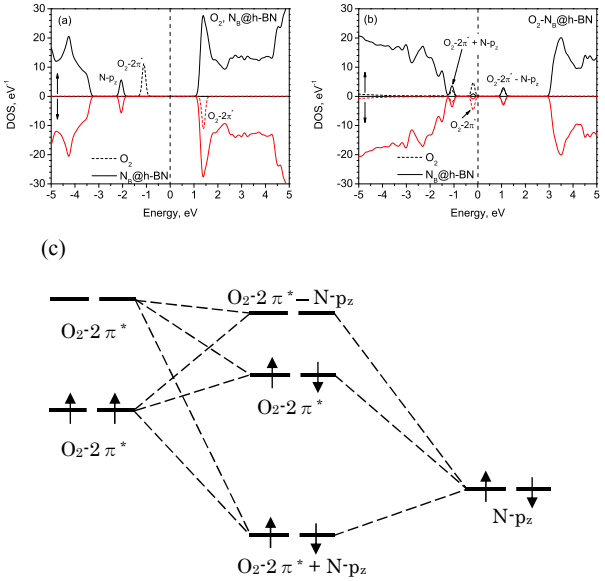

Fig. 6 (a) Spin polarized DOS calculated for N_B@h-BN monolayer (solid line) and free O_2 (dashed line); (b) Partial density of electronic states (PDOS) projected on B and N atoms (solid line) and O_2 (dashed line) calculated for O_2 adsorbed on N_B@h-BN. The location of the Fermi level is indicated by a dashed vertical line at 0 eV. Arrows directed up and down indicate the up-spin and down-spin DOS, respectively. A Gaussian broadening of half-width 0.1 eV has been used. (c) Energy level splitting for interaction of O_2 with N_B@h-BN.

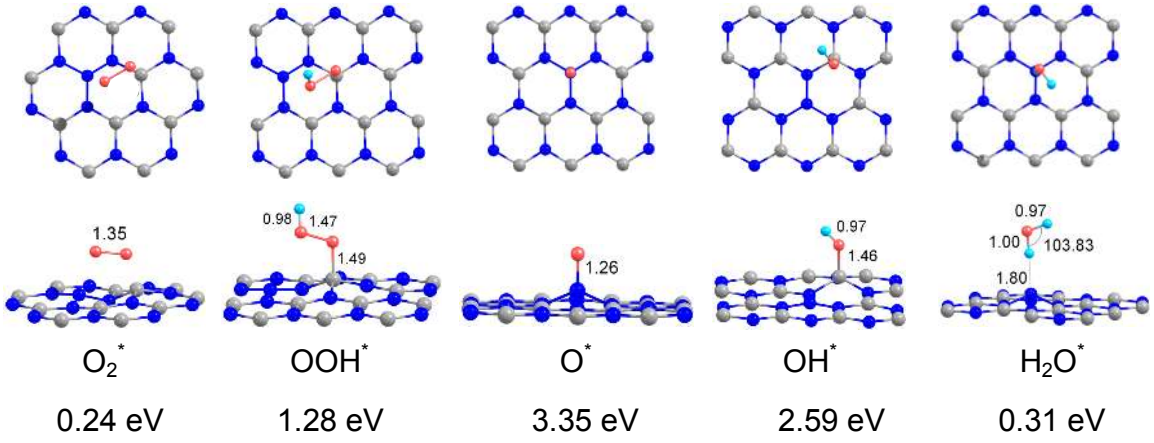

Fig. 5 The most stable configurations of O_2^*, OOH^*, O^*, OH^*, and H_2O^* adsorbed on the h-BN monolayer with N impurity defect. The interatomic distances are given in Angstroms. Adsorbed configurations are marked by asterisk (*). Binding energies of ORR intermediates to N_B@h-BN (with respect to free species) are indicated at the bottom. Only part of the slab is shown.

N_B@h-BN leads to the prominent splitting of the defect N-p_z level due to the strong interaction with the occupied oxygen $2\pi^*$ orbital. Such a splitting results in appearance of the occupied O_2-$2\pi^*$ + N-p_z component just above the edge of the valence band and unoccupied O_2-$2\pi^*$ - N-p_z component above the Fermi level in PDOS, as it is shown in Fig. 6a. In addition interaction of O_2 with N_B defect leads to the partial population of the down-spin O_2-$2\pi^*$ orbital due to depopulation of the N-p_z orbital. Figure 6c schematically represent the energy level splitting due to interaction of O_2 with N_B@h-BN. Partial population of the antibonding $2\pi^*$ orbital of O_2 due to the charge transfer from the surface defect is responsible for the catalytic activation of the adsorbed oxygen and stretching of the O–O bond. According to the Bader analysis, the charge localized on the adsorbed O_2 is -0.94e, where e is an elementary charge. Such mechanism of the charge-transfer-mediated activation of O_2 has been intensively studied for O_2 adsorbed on metal clusters; see, *e.g.*, refs. 44,49,51,73–79 and references therein.

The hydroperoxyl OOH intermediate binds to the B atom nearby the N impurity on the surface. The theoretical value of the binding energy of OOH to N_B@h-BN is 1.28 eV, which is close to the theoretical value of 1.06 eV reported for OOH adsorbed on the Pt(111) surface.[80] The calculated O−O bond length in the supported OOH^* is 1.47 Å. The weakening of the O−O bond should promote dissociation of OOH^* onto O^* and OH^* fragments.

Competition between O−O bond breaking in O_2^* and OOH^* can define the favorable path of ORR. However, before considering dissociation of O_2^* and OOH^* we study independent adsorption of ORR intermediates on N_B@h-BN. Thus, we have found that oxygen atom adsorbs on top of the N impurity with the binding energy of 3.35 eV (referenced to atomic oxygen). It is interesting that this value is very close to the calculated,[26,80] 3.11 - 3.68 eV, and experimentally determined,[81] 3.68 eV, binding energies of oxygen atom on the Pt(111) surface. Figure 5 demonstrates that OH intermediate adsorbs on top of the B atom nearest to the N impurity. The calculated binding energy of OH^* to the surface is 2.59 eV. Previous DFT calculations of OH adsorption on the Pt(111) surface performed with the use of Perdew, Burke and Ernzerhof (PBE)[82] functional led to $E_b(OH/Pt(111))$ = 2.26 eV.[80] DFT calculations using the hybrid Becke-type three-parameter exchange functional[83] paired with the gradient-corrected Lee, Yang and Parr correlation functional[84,85] (B3LYP) performed on a 35 atom Pt cluster (Pt_{35}) imitating Pt(111) surface led to $E_b(OH/Pt(111))$ = 2.06 eV.[86] Finally, we have found that the water molecule adsorbs on top of N impurity in the geometry configuration where the OH bond oriented perpendicular to the surface. The calculated binding energy of H_2O^* to N_B@h-BN is 0.31 eV. B3LYP DFT calculations of H_2O adsorption on Pt(111) surface give $E_b(H_2O/Pt(111))$ = 0.60 eV;[26] while PBE DFT approach predicts $E_b(H_2O/Pt(111))$ = 0.22 eV.[80] The determined experimental values of $E_b(H_2O/Pt(111))$ to be 0.43 - 0.65 eV.[87]

The obtained results are amazing. The energetics of O_2, OOH, O, OH and H_2O adsorption on N_B@h-BN under vacuum conditions is similar to those known for Pt(111) catalyst. Therefore one can suggest that N rich h-BN monolayer can be (under certain conditions that we discuss below) an effective catalyst for ORR, with the catalytic properties similar to platinum. Thus chemically inert h-BN monolayer can be functionalized by doping. There is however considerable difference between ORR processes on N_B@h-BN and Pt(111) surfaces.

In the case of N_B@h-BN system the active cite for ORR is a point defect (N impurity), while for the Pt(111) catalyst it is an extended surface. Therefore, in the case of N_B@h-BN system one should take into account destructive or cooperative interaction between ORR intermediates adsorbed in the vicinity of point defect; while in the case of Pt(111) surface it is possible to operate with the binding energies of ORR intermediates adsorbed independently. That becomes clear if one consider O_2 dissociation on N_B@h-BN. As it was shown above, the most favorable position for O^* on N_B@h-BN is atop of N impurity. When molecular O_2^* dissociates on the N_B@h-BN, one of the oxygen atoms can occupy the energetically favorable position atop of N_B, but another one occupies energetically unfavorable position, bridging B and N atoms nearby the N_B impurity, as it is shown in Fig. 7a. Therefore, the binding energy of two oxygen atoms formed after O_2^* dissociation on N_B@h-BN is smaller than the doubled binding energy of a single O^* on N_B@h-BN. The similar situation occurs upon dissociation of OOH^* on N_B@h-BN, where the resulting products O^* and OH^* are competing for the best position nearby the point defect, as it is shown in Fig. 7b.

Our calculations demonstrate that dissociation of O_2^* on N_B@h-BN is not favorable energetically: the binding energy of 2 O^* on N_B@h-BN is -0.24 eV with respect to free O_2. On the other hand dissociation of OOH^* on N_B@h-BN is energetically favorable process. In the case of ORR on the Pt(111) surface the reaction can occur via O_2 dissociation and OOH association mechanisms, although OOH association mechanism is favorable.[26] However, in the case of h-BN based catalyst with N_B active center only OOH association mechanism of ORR can occur, while the dissociation mechanism is forbidden energetically.

Similar mechanism of self-influence of two ORR intermediates adsorbed on a single catalytic center takes place for 2 OH^* and 2 H_2O^*. In the case of 2 OH^* system both of OH adsorb in the energetically favorable positions on top of B atoms nearby the N_B impurity, as it is shown in Fig. 7c. This type of adsorption is cooperative - the binding energy of 2 OH^* to N_B@h-BN is 5.49 eV, which is 0.31 eV larger, if compared with the independent adsorption of two OH molecules on different N_B@h-BN centers. Two water molecules adsorb on a single N_B@h-BN center also cooperatively. In this case one of the water molecules adsorbes in the energetically favorable position on top of N_B impurity, while another one interacts via hydrogen bond with the adsorbed H_2O^*, forming water dimer. The binding energy of 2 H_2O^* to a single N_B@h-BN center is 0.78 eV, which is 0.16 eV larger, if compared with the independent adsorption of two non-interacting H_2O.

3.4 Reaction energies

In order to describe the overall energetics and ORR mechanisms on N_B@h-BN we use a model approach introduced by Nørskov *et al* in ref. 23. Information on binding preference and adsorption energies of the ORR intermediates allows one to calculate heats of formation, ΔH_f, along the reaction path.[17,23–26,88–91] The free H_2 and O_2 molecules and N_B@h-BN surface are considered as standard states, i.e., $\Delta H_f(H_2)$=0, $\Delta H_f(O_2)$=0, and $\Delta H_f(N_B$@h-BN)=0. This reference set simplifies the consideration of the ORR mechanisms: the reaction starts from the free H_2 and O_2 and goes to the final product – a free H_2O.[24] Figure 8 presents heats of formation, ΔH_f, calculated for the OOH association mechanism of ORR on N_B@h-BN. The following reaction steps are considered:

$$O_2 + * \rightarrow O_2^* \quad (2)$$

$$O_2^* + \left(H^+ + e^-\right) \rightarrow OOH^* \quad (3)$$

$$OOH^* \rightarrow O^* + OH^* \quad (4)$$

$$O^* + \left(H^+ + e^-\right) \rightarrow OH^* \quad (5)$$

$$2OH^* + 2\left(H^+ + e^-\right) \rightarrow 2H_2O^* \quad (6)$$

$$2H_2O^* \rightarrow 2H_2O + *, \quad (7)$$

where asterisk (*) denotes the N_B@h-BN active cite. Heats of formation along the reaction pathway obtained in the approximation of the independent adsorption of ORR intermediates are presented by solid line in Fig. 8. In this approximation we assume that O^*, OH^* and H_2O^* intermediates adsorb on the different N_B@h-BN centers and thus do not interact with each other. Such scenario can occur, for example, if O^* produced after OOH^* dissociation will migrate from the energetically unfavorable position nearby OH^*/N_B@h-BN center (see, Fig. 7b)) to the nearest free N_B@h-BN center, where it can occupy energetically favorable position ontop of the N_B impurity (see, Fig. 5). On the other hand, if ORR occurs on a single point N_B@h-BN center the ORR intermediates can compete for the best position nearby the N_B impurity as it happens for (O^*, OH^*) pair or cooperate in adsorption, as it happens for (OH^*, OH^*) and (H_2O^*, H_2O^*) pairs. The heats of formation, obtained in the approximation of the one-center reaction are presented in Fig. 8 by dashed line.

It is seen from Fig. 8 that ΔH_f goes downhill for all considered steps of ORR, demonstrating that this process is favorable energetically. Moreover, as the binding energies of ORR intermediates on N_B@h-BN are quite similar to those known for Pt(111) surface, the energy diagram for ΔH_f along the reaction pathway reminds that obtained for Pt(111), see, e.g., refs. 24–26. The destructive and cooperative interaction of O^*, OH^* and H_2O^* ORR intermediates in the case of the one-center adsorption slightly modifies the energy diagram of ORR. Thus, it destabilizes the O^*-OH^*/N_B@h-BN configuration after OOH^*

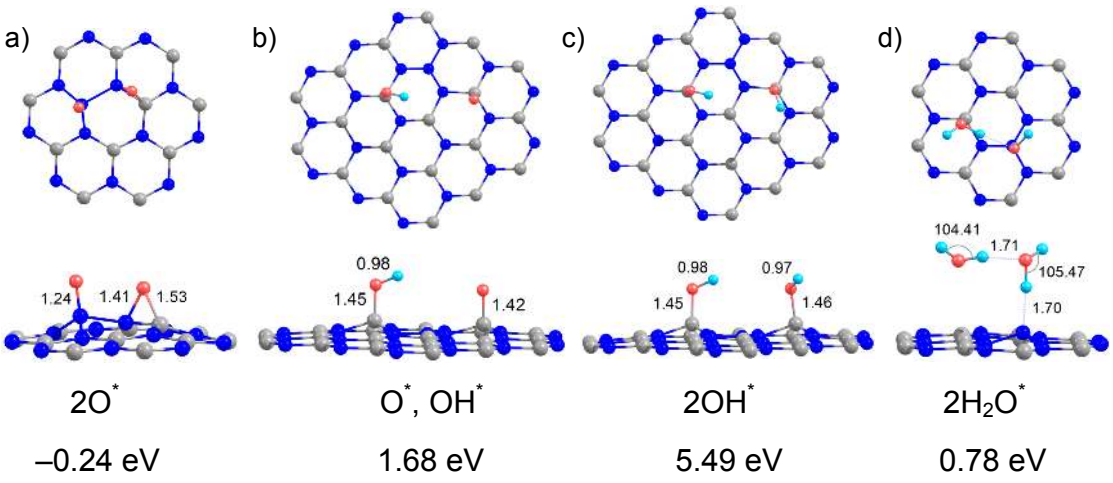

Fig. 7 The optimized configurations of the dissociated (a) $2\,O^*$ and (b) OOH^* as well as coadsorbed (c) $2\,OH^*$ and (d) $2\,H_2O^*$ on N_B@h-BN. The binding energies of (O^*, O^*), (O^*, OH^*), (OH^*, OH^*) and (H_2O^*, H_2O^*) are calculated relatively to free O_2, OOH, $2\,OH$ and $2\,H_2O$ molecules, respectively. The interatomic distances are given in Angstroms and angles are given in degrees. Only part of the slab is shown.

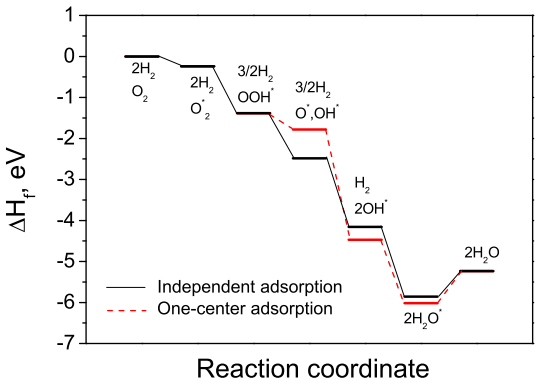

Fig. 8 Heats of formation, ΔH_f, calculated for ORR on N_B@h-BN in the case of (a) intependent adsorption of ORR intermediates (solid line); (b) one-center adsorption of ORR intermediates (dashed line).

dissociation, and slightly stabilizes OH^*-OH^*/N_B@h-BN and H_2O^*-H_2O^*/N_B@h-BN configurations. Although, the destabilization effect of the (O^*, OH^*) pair adsorbed on a single N_B defect is rather noticeable (0.7 eV), it will not affect strongly the overall reaction rate, because the O^*-OH^*/N_B@h-BN configuration is still energetically favorable in comparison with OOH^*/N_B@h-BN. On the other hand the cooperative stabilization of (OH^*, OH^*) and (H_2O^*, H_2O^*) pairs not so large. Therefore, for the sake of simplicity the further analysis of ORR energetics will be performed in the approximation of independent adsorption of ORR intermediates. However, we must note that accurate analysis of ORR energetics might require accounting for destructive and cooperative interaction of intermediates adsorbed on a single reaction center.

Evolution of the uncorrected ΔH_f along the reaction path can serve for a quick and qualitative analysis of the ORR energetics. The accurate investigation of the ORR process requires analysis of the change in a free energy along the reaction pathway, which can be done accounting for the change in entropy, ΔS, during the reaction. It is also necessary to take into account the ZPE corrections, ΔE_{ZPE}:

$$\Delta G_{vac} = \Delta H_f + \Delta E_{ZPE} - T\Delta S, \tag{8}$$

where G_{vac} is the free energy in vacuum and T is the temperature.

In the present work the entropy has been calculated for the free molecules in the ideal gas approximation[92] and has been put to 0 for the molecules adsorbed on the catalytic surface. This is a good approximation, because molecule loses the translational and rotational degrees of freedom upon adsorption. Namely these degrees of freedom make largest contribution to the total entropy. Small corrections to entropic part can arise if one take into account vibrational degrees of freedom of the adsorbed intermediates, however such contributions to the total entropy is small and can be neglected. Note, that in the approximation described above the change in entropy along the reaction pathway does not depend on the type of catalyst or surface. Therefore, entropic corrections can be easily tabulated. The zero-point energy has been calculated by summing vibrational frequencies ω_ν over all normal modes ν:

$$E_{ZPE} = \frac{1}{2}\sum_{\nu}\hbar\omega_\nu. \tag{9}$$

In order to simulate realistic electrochemical conditions it is

also necessary to take into account influence of water environment on the ORR process, which can be included by adding the corresponding energy correction, ΔE_{water}, to the free energy:

$$\Delta G_{water} = \Delta G_{vac} + \Delta E_{water}. \quad (10)$$

Corrections ΔE_{water} have been calculated using the first principles molecular dynamics (FPMD) simulations accounting for water explicitly. We have added 48 water molecules to the system which corresponds to the normal water density in the given simulation cell and performed FPMD simulations for the Nosé-Parrinello-Rahman NPT ensemble of particles keeping constant the number of particles with temperature controlled by means of a Nosé-Hoover thermostat[93,94] and pressure controlled by the Parrinello-Rahman method.[95] A total FPMD simulation has been performed at 300 K for 10 ps with an initial equilibration time of 5 ps. The total energy of the system has been averaged, and ΔE_{water} has been calculated as a difference in heats of formation of ORR intermediates with and without water environment.

Water considerably stabilizes the adsorbed ORR intermediates that can form hydrogen bonds. Figure 9 demonstrates snapshot of FPMD run for O_2^* surrounded by water molecules (only part of the slub is shown). It is seen from Fig. 9 that several water molecules located in the vicinity of O_2^* form hydrogen bonds with the adsorbed oxygen molecule. Formation of the hydrogen bonds results in considerable stabilization of O_2^* on N_B@h-BN. Thus, for example, explicit accounting for water results in increase of the binding energy of O_2 to N_B@h-BN from 0.24 eV to 0.96 eV. Therefore, ΔE_{water}, is one of the very important corrections to the free energy of the system.[80] Interaction of O_2^* with the water molecules results in additional activation of the adsorbed oxygen and increase in the O−O bond length. Figure 9 demonstrates that the O−O bond in O_2^* increases from 1.35 Å for oxygen adsorbed on N_B@h-BN under the vacuum conditions (thick dashed line), to 1.39 Å for O_2^* in water (thick solid line). Similar effect has been discussed in ref. 17.

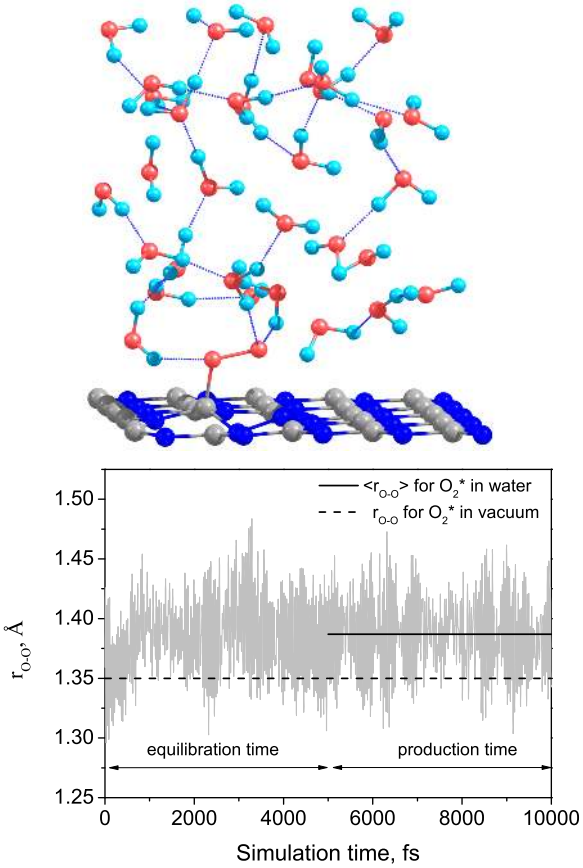

Fig. 9 Top: Snapshot of FPMD run for O_2^* surrounded by water molecules (only part of the slub is shown). Formation of the hydrogen bonds results in stabilization of O_2^*. Bottom: The O−O bond length, $r_{O\text{-}O}$, in the adsorbed oxygen as a function of simulation time (thin line), time averaged $<r_{O\text{-}O}>$ calculated for O_2^* in water (thick solid line), and the O−O bond length in O_2^* adsorbed under the vacuum conditions (thick dashed line).

Figure 10a presents energy diagram calculated for the OOH association mechanism of ORR on N_B@h-BN. Heats of formation, ΔH_f, without ZPE and solvent corrections are presented by solid lines, while changes in free energy, ΔG_{water}, accounting for entropy, zero-point energy and solvent effects are presented by dashed lines.

Let us consider how ΔE_{ZPE}, $-T\Delta S$, and ΔE_{water} corrections affect the energetics of the ORR process. Solid line in Fig. 10b presents the sum of the ZPE and entropic contributions, $\Delta E_{ZPE} - T\Delta S$ to the free energy along the reaction pathway, while dashed line presents the contribution of the solvent corrections, ΔE_{water}. It is seen from Fig. 10b that ZPE and entropy corrections are positive and hence destabilize the system; while accounting for a water environment results in considerable stabilization of ORR intermediates. The absolute values of energy corrections are large. However, as it is seen from Fig. 10b the destabilizing, $\Delta E_{ZPE} - T\Delta S$, and stabilizing, ΔE_{water}, corrections partly cancel each other. Thus the total contribution of $\Delta E_{ZPE} - T\Delta S + \Delta E_{water}$ corrections to the free energy is relatively small (line with dots in Fig. 10b). Therefore, in order to reproduce the energetics of the ORR process correctly it is important to take into account zero-point energy, entropy and solvent effects simultaneously. Each of these effects taken separately is rather large and can considerably contribute to the free energy. Thus accounting for example only for ΔE_{water} term can result in considerable overestimation of the binding energies of ORR intermediates, while neglecting the solvent corrections can result in considerable destabilization of ORR intermediates.

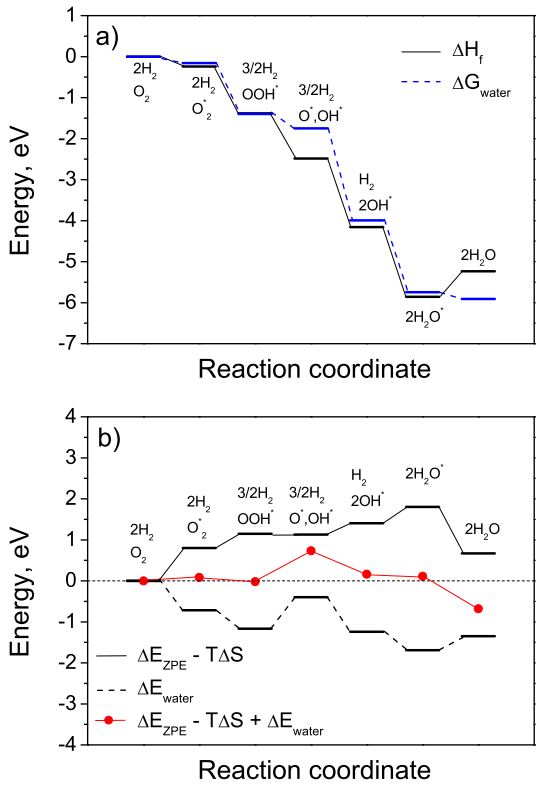

Fig. 10 Energy diagram for ORR on N_B@h-BN. (a) Uncorrected heats of formation ΔH_f calculated in the approximation of the independent adsorption of ORR intermediates (solid line); free energy, ΔG_{water}, corrected for zero-point energy and solvent effect (dashed line). (b) The destabilizing, $\Delta E_{ZPE} - T\Delta S$, (solid line) and stabilizing, ΔE_{water}, (dashed line) energy corrections along the ORR path. Sum of all considered energy corrections, $\Delta E_{ZPE} - T\Delta S + \Delta E_{water}$ (dots).

4 Conclusions

In summary, the present theoretical study demonstrates that inert h-BN material can be functionalized and become catalytically active for ORR. We have investigated the binding preference and catalytic activation of O_2 adsorbed on the surface of the pristine and defected h-BN monolayer as well as the various adsorption sites at the H-terminated edges of h-BN nanoribbon. We have demonstrated that the N impurity defect on the surface of the h-BN monolayer can be a good candidate for the active center of ORR. We have shown that the adsorption energies of O_2, O, OH, OOH, and H_2O on N_B@h-BN are quite similar to those known for adsorption of ORR intermediates on Pt(111) surface. An important role of entropy contribution, zero-point energy corrections and solvent effects on adsorption energies of O_2 and ORR intermediates is discussed. We have demonstrated that ΔE_{ZPE}, $-T\Delta S$, and ΔE_{water} terms in the expression for the free energy can partly cancel each other. Therefore, in order to reproduce the energetics of the ORR process correctly it is important to take into account ZPE, entropy and solvent effects simultaneously. The uncorrected heats of formation, ΔH_f, can be considered as a good initial approximation for simple analysis of the ORR energetics on N_B@h-BN.

On the basis of free energy analysis we have suggested that N-doped h-BN monolayer can demonstrate catalytic properties for ORR. However in order to use such a catalist on the cathode of a fuel cell it is necessary to provide an electron transport to the catalytically active center. As it was already discussed, the electron transport phenomenon can occur if h-BN monolayer is deposited on a surface of some transition metals, such as, Ni(111) or Au(111). This suggestion requires further investigation that goes far beyond the aims of the present study. The study on adsorption of O_2 and other ORR intermediates on the metal supported h-BN monolayer will be given in a further publication. We hope that our work will stimulate further experimental and theoretical study of the considered phenomena.

Acknowledgements

This work was supported by Elements Science and Technology Project of Ministry of Education, Culture, Sports, Science and Technology, Japan (MEXT) on "Nano-hybridized Precious-metal-free Catalysts for Chemical Energy Conversion"; MEXT program "Elements Strategy Initiative to Form Core Rersearch Center" (since 2012); and the JSPS Grant-in-Aid for Scientific Research C. The computations were partly performed using the Research Center for Computational Science, Okazaki, Japan.

References

1 N. P. Brandon, S. Skinner and B. C. H. Steele, *Annu. Rev. Mater. Res.*, 2003, **33**, 183–213.
2 *Fuel Cell Catalysis: A Surface Science Approach*, ed. M. T. M. Koper, John Willy & Sons, Inc., 2009.
3 A. Rabis, P. Rodriguez and T. J. Schmidt, *ACS Catalysis*, 2012, **2**, 864–890.
4 L. Xiong, A. M. Kannan and A. Manthiram, *Electrochem. Comm.*, 2002, **4**, 898 – 903.
5 T. Wadayama, N. Todoroki, Y. Yamada, T. Sugawara, K. Miyamoto and Y. Iijama, *Electrochem. Comm.*, 2010, **12**, 1112–1115.
6 V. R. Stamenkovic, B. Fowler, B. S. Mun, G. Wang, P. N. Ross, C. A. Lucas and N. M. Marković, *Science*, 2007, **315**, 493–497.
7 J. Zhang, Y. Mo, M. B. Vukmirovic, R. Klie, K. Sasaki and R. R. Adzic, *J. Phys. Chem. B*, 2004, **108**, 10955–10964.
8 H. Zhu, X. Li and F. Wang, *Int. J. Hydrogen Energy*, 2011, **36**, 9151 – 9154.
9 R. Kothandaraman, V. Nallathambi, K. Artyushkova and S. C. Barton, *Appl. Catal. B: Env.*, 2009, **92**, 209 – 216.

10 G. Wu, K. L. More, C. M. Johnston and P. Zelenay, *Science*, 2001, **332**, 443–447.
11 R. A. Sidik, A. B. Anderson, N. P. Subramanian, S. P. Kumaraguru and B. N. Popov, *J. Phys. Chem. B*, 2006, **110**, 1787–1793.
12 J.-i. Ozaki, T. Anahara, N. Kimura and A. Oya, *Carbon*, 2006, **44**, 3358 – 3361.
13 J.-i. Ozaki, N. Kimura, T. Anahara and A. Oya, *Carbon*, 2007, **45**, 1847–1853.
14 T. Ikeda, M. Boero, S.-F. Huang, K. Terakura, M. Oshima and J.-i. Ozaki, *J. Phys. Chem. C*, 2008, **112**, 14706–14709.
15 S.-F. Huang, K. Terakura, T. Ozaki, T. Ikeda, M. Boero, M. Oshima, J.-i. Ozaki and S. Miyata, *Phys. Rev. B*, 2009, **80**, 235410.
16 T. Ikeda, M. Boero, S.-F. Huang, K. Terakura, M. Oshima, J.-i. Ozaki and S. Miyata, *J. Phys. Chem. C*, 2010, **114**, 8933–8937.
17 L. Yu, X. Pan, X. Cao, P. Hu and X. Bao, *J. Catal.*, 2011, **282**, 183–190.
18 L. Zhang and Z. Xia, *J. Phys. Chem. C*, 2011, **115**, 11170–11176.
19 L. Qu, Y. Liu, J.-B. Baek and L. Dai, *ACS Nano*, 2010, **4**, 1321–1326.
20 X. Wang, Z. Hou, T. Ikeda, S.-F. Huang, K. Terakura, M. Boero, M. Oshima, M.-a. Kakimoto and S. Miyata, *Phys. Rev. B*, 2011, **84**, 245434.
21 X. Wang, C. Zhi, L. Li, H. Zeng, C. Li, M. Mitome, D. Golberg and Y. Bando, *Adv. Mater.*, 2011, **23**, 4072–4076.
22 X. Wang, A. Pakdel, C. Zhi, K. Watanabe, T. Sekiguchi, D. Golberg and Y. Bando, *J. Phys.: Condens. Matter*, 2012, **24**, 314205.
23 J. K. Nørskov, J. Rossmeisl, A. Logadottir, L. Lindqvist, J. R. Kitchin, T. Bligaard and H. Jónsson, *J. Phys. Chem. B*, 2004, **108**, 17886–17892.
24 T. Jacob, *Fuel Cells*, 2006, **06**, 159–181.
25 J. A. Keith, G. Jerkiewicz and T. Jacob, *ChemPhysChem*, 2010, **11**, 2779–2794.
26 J. A. Keith and T. Jacob, *Angew. Chem. Int. Ed.*, 2010, **49**, 9521–9525.
27 Z. Wu and R. E. Cohen, *Phys. Rev. B*, 2006, **73**, 235116/1–6.
28 F. Tran, R. Laskowski, P. Blaha and K. Schwarz, *Phys. Rev. B*, 2007, **75**, 115131.
29 E. Artacho, D. Sánchez-Portal, P. Ordejón, A. García and J. M. Soler, *Phys. Stat. Sol. (b)*, 1999, **215**, 809–817.
30 J. Junquera, O. Paz, D. Sánchez-Portal and E. Artacho, *Phys. Rev. B*, 2001, **64**, 235111/1–9.
31 J. A. Nelder and R. Mead, *The Computer Journal*, 1965, **7**, 308–313.
32 N. Troullier and J. L. Martins, *Phys. Rev. B*, 1991, **43**, 1993–2006.
33 L. Kleinman and D. M. Bylander, *Phys. Rev. Lett.*, 1982, **48**, 1425–1428.
34 D. Sánchez-Portal, P. Ordejón, E. Artacho and J. M. Soler, *Int. J. Quantum Chem.*, 1997, **65**, 453–461.
35 J. M. Soler, E. Artacho, J. D. Gale, A. García, J. Junquera, P. Ordejón and D. Sánchez-Portal, *J. Phys.: Condens. Matter*, 2002, **14**, 2745–2779.
36 D. Sánchez-Portal, P. Ordejón and E. Canadell, *Structure and Bonding*, 2004, **113**, 103–170.
37 H. J. Monkhorst and J. D. Pack, *Phys. Rev. B*, 1976, **13**, 5188.
38 C. S. Yoo, J. Akella, H. Cynn and M. Nicol, *Phys. Rev. B*, 1997, **56**, 140–146.
39 K. P. Huber and G. Herzberg, *Molecular Spectra and Molecular Structure Constants of Diatomic Molecules*, Van Nostrand Reinhold, New York, 1979.
40 W. S. Benedict, N. Gailar and E. K. Plyler, *J. Chem. Phys.*, 1956, **24**, 1139–1165.
41 J. A. Odutola and T. R. Dyke, *J. Chem. Phys.*, 1980, **72**, 5062–5070.
42 L. A. Curtiss, D. J. Frurip and M. Blander, *J. Chem. Phys.*, 1979, **71**, 2703–2711.
43 X. Xu and W. A. Goddard, *J. Phys. Chem. A*, 2004, **108**, 2305–2313.
44 A. Lyalin and T. Taketsugu, *J. Phys. Chem. C*, 2009, **113**, 12930–12934.
45 A. Lyalin and T. Taketsugu, *AIP Conference Proceedings*, 2009, **1197**, 65–75.
46 A. Lyalin and T. Taketsugu, *J. Phys. Chem. C*, 2010, **114**, 2484–2493.
47 A. Lyalin and T. Taketsugu, *J. Phys. Chem. Lett.*, 2010, **1**, 1752–1757.
48 A. Lyalin and T. Taketsugu, *Faraday Discuss.*, 2011, **152**, 185–201.
49 M. Gao, A. Lyalin and T. Taketsugu, *Catalysts*, 2011, **1**, 18–39.
50 M. Gao, A. Lyalin and T. Taketsugu, *J. Phys. Chem. C*, 2012, **116**, 9054–9062.
51 M. Gao, A. Lyalin and T. Taketsugu, *Int. J. Quantum Chem.*, 2012.
52 A. Lyalin, I. A. Solov'yov, A. V. Solov'yov and W. Greiner, *Phys. Rev. A*, 2003, **67**, 063203.
53 A. Lyalin, I. A. Solov'yov, A. V. Solov'yov and W. Greiner, *Phys. Rev. A*, 2007, **75**, 053201.
54 A. Lyalin, A. V. Solov'yov and W. Greiner, *Phys. Rev. A*, 2006, **74**, 043201.
55 R. Bader, *Atoms in Molecules: A Quantum Theory*, Oxford University Press, New York, 1990.
56 G. Henkelman, A. Arnaldsson and H. Jónsson, *Comput. Mater. Sci.*, 2006, **36**, 354–360.
57 J. Furthmüller, J. Hafner and G. Kresse, *Phys. Rev. B*, 1994, **50**, 15606–15622.
58 H. Zeng, C. Zhi, Z. Zhang, X. Wei, X. Wang, W. Guo, Y. Bando and D. Golberg, *Nano Lett.*, 2010, **10**, 5049–5055.
59 S. Azevedo, J. R. Kaschny, C. M. de Castilho and F. de Brito Mota, *Eur. Phys. J. B*, 2009, **67**, 507–512.
60 J. Zhou, Q. Wang, Q. Sun and P. Jena, *Phys. Rev. B*, 2010, **81**, 085442.
61 L. Britnell, R. V. Gorbachev, R. Jalil, B. D. Belle, F. Schedin, M. I. Katsnelson, L. Eaves, S. V. Morozov, A. S. Mayorov, N. M. R. Peres, A. H. Castro Neto, J. Leist, A. K. Geim, L. A. Ponomarenko and K. S. Novoselov, *Nano Lett.*, 2012, **12**, 1707–1710.
62 A. B. Preobrajenski, A. S. Vinogradov and N. Mårtensson, *Surf. Sci.*, 2005, **582**, 21–30.
63 R. Laskowski, P. Blaha and K. Schwarz, *Phys. Rev. B*, 2008, **78**, 045409/1–10.
64 W. Orellana and H. Chacham, *Phys. Rev. B*, 2001, **63**, 125205.
65 A. A. Kuzubov, M. V. Serzhantova, A. S. Fedorov, F. N. Tomilin and T. A. Kozhevnikova, *JETP Lett.*, 2011, **93**, 335–338.
66 V. Solozhenko, A. Lazarenko, J.-P. Petitet and A. Kanaev, *J. Phys. Chem. Solids*, 2001, **62**, 1331 – 1334.
67 *Inorganic Chemistry*, ed. N. Wiberg, A. F. Holleman and E. Wiberg, Academic Press, 2001.
68 J. L. Gland, B. A. Sexton and G. B. Fisher, *Surf. Sci.*, 1980, **95**, 587–602.
69 C. Campbell, G. Ertl, H. Kuipers and J. Segner, *Surf. Sci.*, 1981, **107**, 220–236.
70 P. D. Nolan, B. R. Lutz, P. L. Tanaka, J. E. Davis and C. B. Mullins, *J. Chem. Phys.*, 1999, **111**, 3696–3704.
71 A. Eichler and J. Hafner, *Phys. Rev. Lett.*, 1997, **79**, 4481–4484.
72 L. Qi, J. Yu and J. Li, *J. Chem. Phys.*, 2006, **125**, 054701.
73 H. Häkkinen and U. Landman, *J. Am. Chem. Soc.*, 2001, **123**, 9704–9705.
74 L. D. Socaciu, J. Hagen, T. M. Bernhardt, L. Wöste, U. Heiz, H. Häkkinen and U. Landman, *J. Am. Chem. Soc.*, 2003, **125**, 10437–10445.
75 H. Häkkinen, S. Abbet, A. Sanchez, U. Heiz and U. Landman, *Angew. Chem. Int. Ed.*, 2003, **42**, 1297–1300.
76 B. Yoon, H. Häkkinen and U. Landman, *J. Phys. Chem. A*, 2003, **107**, 4066–4071.
77 R. Coquet, K. L. Howard and D. J. Willock, *Chem. Soc. Rev.*, 2008, **37**, 2046–2076.
78 X. Ding, Z. Li, J. Yang, J. G. Hou and Q. Zhu, *J. Chem. Phys.*, 2004, **120**, 9594–9600.
79 E. Fernández, P. Ordejón and L. C. Balbás, *Chem. Phys. Lett.*, 2005, **408**, 252–257.
80 Y. Sha, T. H. Yu, Y. Liu, B. V. Merinov and W. A. Goddard, *J. Phys. Chem. Lett.*, 2010, **1**, 856–861.
81 D. H. Parker, M. E. Bartram and B. E. Koel, *Surf. Sci.*, 1989, **217**, 489 – 510.

82 J. P. Perdew, K. Burke and M. Ernzerhof, *Phys. Rev. Lett.*, 1996, **77**, 3865–3868.
83 A. D. Becke, *Phys. Rev. A*, 1988, **38**, 3098–3100.
84 C. Lee, W. Yang and R. G. Parr, *Phys. Rev. B*, 1988, **37**, 785–789.
85 R. G. Parr and W. Yang, *Density-Functional Theory of Atoms and Molecules*, Oxford University Press, Oxford, New York, 1989.
86 T. Jacob and W. A. Goddard, *ChemPhysChem*, 2006, **7**, 992–1005.
87 G. B. Fisher and J. L. Gland, *Surf. Sci.*, 1980, **94**, 446–455.
88 J. Rossmeisl, J. K. Nørskov, C. D. Taylor, M. J. Janik and M. Neurock, *J. Phys. Chem. B*, 2006, **110**, 21833–21839.
89 P. Vassilev and M. T. M. Koper, *J. Phys. Chem. C*, 2007, **111**, 2607–2613.
90 K.-Y. Yeh and M. J. Janik, *Journal of Computational Chemistry*, 2011, **32**, 3399–3408.
91 V. Tripković, E. Skúlason, S. Siahrostami, J. K. Nørskov and J. Rossmeisl, *Electrochimica Acta*, 2010, **55**, 7975–7981.
92 D. A. McQuarrie and J. D. Simon, *Molecular Thermodynamics*, University Science Books, 1999.
93 S. Nosé, *J. Chem. Phys.*, 1984, **81**, 511–519.
94 W. G. Hoover, *Phys. Rev. A*, 1985, **31**, 1695–1697.
95 M. Parrinello and A. Rahman, *Journal of Applied Physics*, 1981, **52**, 7182–7190.